KAZUE TAKAHASHI

RESPONSE OF ENERGETIC PARTICLES TO MAGNETOSPHERIC ULTRA-LOW-FREQUENCY WAVES

Ultra-low-frequency (ULF) waves in the space physics context are the lowest-frequency plasma waves propagating in the Earth's magnetosphere. Although the propagation of the waves is explained in magnetohydrodynamic (MHD) theory, excitation of the waves involves not only MHD but also kinetic processes. In this article, we describe how *in situ* magnetic field and particle measurements can be used to distinguish the basic properties of ULF waves, including the azimuthal wave number of the standing wave structure and the propagation direction. Examples are taken from observations with the AMPTE/CCE spacecraft.

INTRODUCTION

A long time ago it was realized that the geomagnetic field as observed on the ground exhibits small-amplitude oscillations with a period of a few minutes.[1] Since then, the phenomenon has attracted many researchers and has been called by several different names, including geomagnetic micropulsations, magnetic pulsations, ultra-low-frequency (ULF) pulsations (i.e., frequencies lower than 3 Hz), or ULF waves. In 1954, Dungey[2] predicted that the oscillations originate in the magnetosphere as magnetohydrodynamic (MHD) waves. As soon as satellite measurements of the Earth's magnetic fields became available, this theoretical prediction was confirmed.[3] Nowadays, magnetometers on scientific satellites routinely detect ULF pulsations in the magnetosphere.

While the propagation of ULF waves in the magnetosphere can be explained in terms of MHD, the mechanisms for exciting the waves are not fully understood. Thus a great deal of effort is still being expended, both in observation and in theory, to identify the excitation mechanisms. One class of pulsations can be generated from external sources such as the Kelvin-Helmholtz instability on the magnetopause,[4,5] and other class of pulsations can be generated by plasma instabilities in the magnetosphere.[6,7] However, the basic distinguishing properties of the waves (such as wave number and propagation direction) are not easily determined from observation. One experimental difficulty is that ULF waves are of large scale, often comparable to the dimension of the magnetosphere itself, while spacecraft measurements are made at one point or perhaps at a half-dozen points in the entire magnetosphere.

One major scientific motivation for studying magnetospheric ULF waves is that a detailed comparison is possible between plasma theory and observation in the magnetospheric environment. Unlike laboratory plasmas, the magnetospheric plasma is free of walls or disturbances from diagnostic tools (spacecraft). In addition, the wave frequency can be very low, so that particle distributions in phase space at different oscillation phases can be experimentally determined. This provides a quantitative basis for testing various theories of plasma instabilities.

In this article we describe how energetic particle data combined with magnetic field data can be used to understand the properties of ULF waves. In some cases, the particles can be treated separately from the bulk of the plasma, and can be used as test particles probing the spatial and temporal structure of ULF pulsations. In that case, the type of wave–particle interactions critically depends on the spatial structure of ULF waves. We show examples of wave–particle interactions from data acquired by the Active Magnetospheric Particle Tracer Explorers/Charge Composition Explorer (AMPTE/CCE) spacecraft and demonstrate that from single spacecraft measurements of particle fluxes we can infer the spatial structure of ULF waves. The organization of this article is as follows: In the following section, the general theory of ULF waves and the behavior of energetic particles are outlined. Then the magnetic field and particle experiments on AMPTE/CCE are described. Finally, examples of ion flux oscillations are illustrated.

STANDING WAVES AND MOTION OF ENERGETIC PARTICLES

Magnetohydrodynamics describes the fluid-like behavior of a plasma at frequencies lower than the ion cyclotron frequency, which is about 1 Hz or higher in the Earth's magnetosphere. Magnetohydrodynamics allows propagation of both compressional waves, called fast-mode waves, and transverse waves, called Alfvén waves. The fast-mode waves propagate across the ambient geomagnetic field and transfer wave energy between different magnetic shells. The Alfvén waves, in contrast, propagate along geomagnetic field lines. Because the ionosphere is a good reflector for Alfvén waves that are incident from the magnetosphere, the energy of plasma and field perturbations propagating in the Alfvén mode is reflected back and forth between the northern and southern ends of geomagnetic field lines. As a conse-

quence, ULF disturbances tend to establish standing Alfvén waves, as was predicted by Dungey.[2] The waves are in a sense analogous to the vibration of a string fixed at both ends. In MHD, the restoring force (tension) is provided by the Maxwell stress of the geomagnetic field.

The two lowest-order modes of the standing waves are illustrated in Figure 1. The fundamental mode has an antinode of field line displacement at the equator. Because the transverse magnetic field perturbation, $\delta B_\perp$, is proportional to the local tilt angle of the displaced field line, $\delta B_\perp$ has a node at the equator. For the second harmonic, the field displacement is null at the equator, while $\delta B_\perp$ has an antinode there. The frequency of a standing Alfvén wave is given approximately by the fundamental frequency $f_A = (\int ds/V_A)^{-1}$, or by its harmonic, where V_A is the Alfvén velocity and ds is the line element along a geomagnetic field line, and the integral is taken over a return path from the southern end to the northern end of the field line. The Alfvén velocity is given by $V_A = B/(4\pi\rho)^{1/2}$, where B is the field line intensity and ρ is the plasma mass density. Therefore, the standing wave frequency, f_A, depends on both B and ρ, as well as on the length of the geomagnetic field line. It must be mentioned that waves excited in a hot plasma often exhibit a strong compressional component. In that case, the waves cannot be a pure Alfvén mode. There is strong coupling, however, between compressional waves and Alfvén waves, and the wave reflection at the ionosphere leads to standing structures even for the mixed-mode waves.[8]

Very clear evidence for the standing waves has been obtained from dynamic spectra of magnetic field measurements from Earth-orbiting satellites.[9] Example spectra from four consecutive inbound passes of AMPTE/CCE are shown in Figure 2. Power spectral density relative to the background, which is defined by a best-fit second-order polynomial to the original spectrum, is displayed by color, with blue, green, yellow, and red indicating increasingly high power levels. Each color-coded spectrum shows a frequency structure of the azimuthal magnetic field oscillation as a function of geocentric distance, L, measured in units of Earth radii (R_E). The clearly visible red traces correspond to the fundamental and the third-harmonic standing Alfvén waves on the local geomagnetic field line. The frequency decrease with L is caused by a rapid decrease of magnetic field magnitude with distance.

In addition to the magnetic pulsation, an electric field oscillation given by $\mathbf{E} = -\mathbf{V} \times \mathbf{B}$ accompanies an Alfvén wave, where $\mathbf{E}$ is the electric field, $\mathbf{V}$ is the plasma bulk velocity, and $\mathbf{B}$ is the magnetic field. Because measurements of ULF electric fields are more difficult than magnetic field measurements, the presence of a ULF wave is usually determined by magnetic field experiments.

Many magnetic pulsations accompany particle flux oscillation.[10–12] To understand how the flux oscillations occur, we start with the motion of individual particles, which is given by

$$M\frac{dv}{dt} = q[\mathbf{E} + (\mathbf{v} \times \mathbf{B})] , \qquad (1)$$

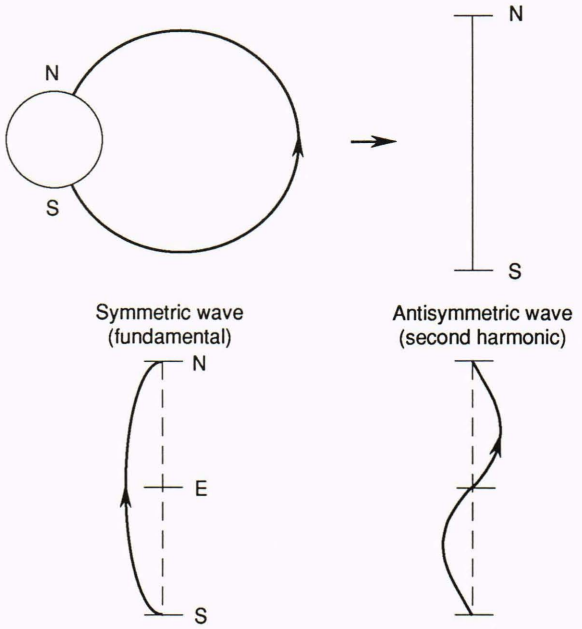

Figure 1. Schematic of standing waves on a geomagnetic field line. For simplicity, the curved geomagnetic field line is represented by a straight field string with ends fixed. The fundamental mode has maximum displacement at the equator. The second harmonic has null displacement at the equator.

where M is the particle mass, $\mathbf{v}$ is the particle velocity, and q is the electric charge. In the absence of temporal variations in $\mathbf{E}$ and $\mathbf{B}$, particle motion in a dipole geomagnetic field is composed of gyromotion, bounce motion, and drift motion of the guiding center, as illustrated in Figure 3. The circular motion of particles about the magnetic field that arises from the magnetic part of the Lorenz force $q\mathbf{v} \times \mathbf{B}$ is called the gyromotion. The period of the gyromotion (called the gyroperiod), $2\pi M/qB$, does not depend on energy for nonrelativistic particles. For a magnetic field of 100 nT, which is typical at geostationary orbit, the proton gyroperiod is 0.7 s. The guiding center is the instantaneous center of the gyromotion, and its bounce and drift motions arise from the dipole configuration of the geomagnetic field. The former arises because the magnetic field lines converging at higher latitudes push particles back to the equator. The latter arises because the curvature of the field lines gives a centrifugal force for the guiding center and also because the radial gradient of $\mathbf{B}$ leads to displacement of the guiding center at consecutive gyrations. The speed of the guiding center motions depends on particle energy. For example, the bounce period and the drift period (the time interval that it takes a guiding center to complete an azimuthal rotation about the Earth) at geostationary altitude are ~120 s and ~8 h for 10-keV protons and ~40 s and ~50 min for 100-keV protons.

In the presence of field perturbations, these particle motions are modified. If we could trace the orbits of individual particles, then we could determine the field perturbations. There is no experimental technique, however, to trace individual particles in the magnetosphere. Instead, particle detectors measure the directional dif-

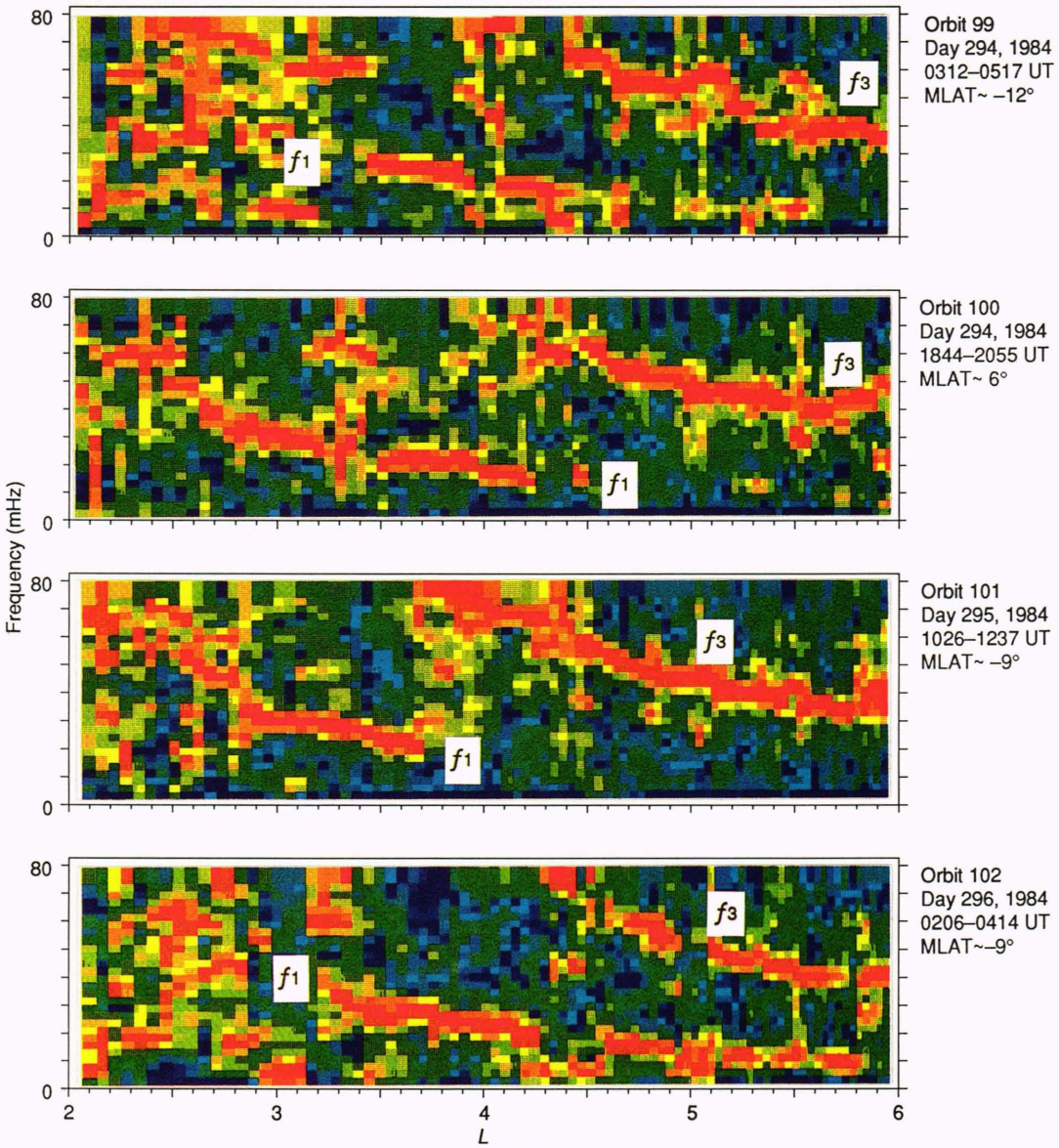

Figure 2. Color-coded dynamic power spectra of AMPTE/CCE magnetic field data for four consecutive inbound passes in the dayside magnetosphere. The red portion of the spectra represents spectral peaks. (Reprinted, with permission, from Ref. 15: © 1990 American Geophysical Union.)

ferential flux, dJ/dW, at a single point in space, where W is the kinetic energy of the particles, and J is the integral flux over energy. Consequently, theory has been developed to describe wave–particle interactions in terms of dJ/dW or the phase space density, f, which is related to dJ/dW by

$$f = \frac{M^2}{2W}\frac{dJ}{dW} \quad . \tag{2}$$

If we assume f to be a function of the phase space coordinates $\mathbf{X}$ and time t, and if we also assume perturbations in f to be small, the Liouville theorem that f is constant along the orbit of an individual particle in phase space gives

$$\delta f(\mathbf{X}, t) \equiv f(\mathbf{X}, t) - f(\mathbf{X}, t_0)$$

$$\approx -\frac{\partial f}{\partial \mathbf{X}} \cdot \delta\mathbf{X} \quad , \tag{3}$$

where δf is the perturbation in f measured at some point in the the phase space, t_0 is a reference time, and $\delta\mathbf{X}$ is the change in the phase space coordinates experienced by individual particles between t_0 and t.[13] Usually, $\delta\mathbf{X}$ is represented by phase space variables such as δW and $\delta\alpha$, where the pitch angle, α, is the instantaneous angle between the particle velocity vector and the magnetic field. Equations 2 and 3 formally connect observation and theory. In individual cases, the form of $\delta\mathbf{X}$ depends

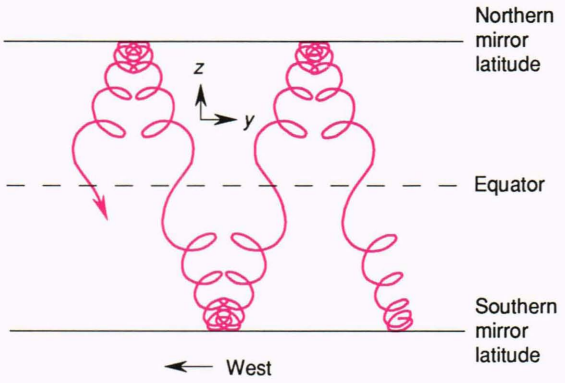

Figure 3. Schematic of the motion of ions in the Earth's dipole field. The motion consists of gyration about the magnetic field and drift-bounce motion of the gyrocenter. In the absence of an electric field, ions drift westward.

on the dominant electromagnetic components and the spatial structure of the ULF wave. Mathematically, $\delta\mathbf{X}$ is expressed as an integral of wave-induced perturbations in energy, guiding center location, etc., over the unperturbed orbit of individual particles.

Because the modulation in f represents effects accumulated over a particle orbit, we can infer the spatial structure of ULF waves from the analysis of particle flux modulations seen at a single point in space. In the magnetospheric region where the field is dominated by the Earth's dipole field, the symmetry of the wave field about the magnetic equator and the wave number in the azimuthal direction are the most important parameters for determining the origin of the waves. Therefore, to infer the spatial structure from particle data, we usually assume ULF waves to have the form $g(z)e^{i(m\phi-\omega t)}$, where $g(z)$ is the structure along the ambient magnetic field, m is the azimuthal wave number, ϕ is azimuth in dipole coordinates, and ω is the angular frequency.

CCE INSTRUMENTATION

In addition to the above theoretical aspects, knowledge of experiments is necessary to fully understand the response of energetic particles to ULF waves. This section describes the magnetometer and a particle detector on the AMPTE/CCE spacecraft. These instruments are the basis for the observations presented in the section entitled Examples of Particle Flux Modulations.

Spacecraft Properties

The spacecraft is in a low-inclination (4.8°) elliptical orbit with its apogee at 8.8 R_E, its perigee at 1.2 R_E, and an orbital period of 15.6 h. The great advantage of such an orbit is that a wide range of L values is covered. (L values are the designation of field lines by their distance in Earth radii from the center of the Earth to the point where they cross the geomagnetic equator.) In addition, AMPTE/CCE covers a reasonably wide range of geomagnetic latitude (±16°), which is important for observing the field-aligned structure of ULF waves. The spacecraft is spin stabilized with its spin axis maintained at 10° to 30° of the Sun–Earth line. The spin period is about 6 s.

Magnetic Field Experiment

This experiment consists of triaxial flux gate magnetometer sensors mounted on a 2.3-m boom.[14] It has 13-bit amplitude resolution in each of the seven automatically switchable dynamic ranges. The sampling rate is 8.06 vector samples per second. These characteristics are more than adequate for studying ULF pulsations, which typically have an amplitude exceeding 1% of the ambient field intensity and periods longer than 10 s. The magnetic field measurements are sensitive to ULF pulsations occurring at distances as close as $L = 2\ R_E$,[15] if the data are adequately filtered to avoid strong interference at the spin frequency of the satellite and at its harmonics.

Medium Energy Particle Analyzer

The Medium Energy Particle Analyzer (MEPA) is one of the three particle experiments on board CCE.[16] It measures the fluxes of medium-energy ions with a time-of-flight (TOF) head and an ion head. The TOF head measures the particle energy with a solid state detector (SSD), and the particle speed from the time differences between the time particles pass thin foils and the time they arrive at the SSD. Thus the TOF head distinguishes different ion species. The ion head measures particle energy by a SSD but cannot measure the time of flight. Data from the ion head are usually used in our study, however, because of their favorable energy steps and time resolutions. There are 10 energy passbands for the ion head starting at 25 to 34 keV. Usually a few bands at low energies (ECH0, ECH1, . . . , ECH4) provide sufficiently high counting rates for identifying modulations associated with magnetic pulsations. In addition, we have extensively used data from the front microchannel plate (MCP1) of the TOF head. The MCP1 measures secondary electrons emitted from the front foil as an energetic ion passes it. Although MCP1 gives only a rough measure of ion flux intensity above about 10 keV, its high counting statistics make it useful for finding fine pitch angle–time structures in ion flux modulations.

Pitch angle distribution for ions can be measured using the spin of the satellite (the detector look direction is perpendicular to the spin axis). Because the spin axis is nearly parallel to the geomagnetic equator, almost the full range of pitch angle can be covered when the satellite is in the region dominated by the dipole geomagnetic field of the Earth. This is one major advantage of using the MEPA. A thirty-two-sector pitch angle distribution from the ion head is available at a time resolution of 6 to 24 s, depending on the energy band. This ensures that several "snapshots" of pitch angle distribution are available during one cycle of a ULF wave. This is another advantage of using the MEPA.

EXAMPLES OF PARTICLE FLUX MODULATIONS

This section will illustrate some individual cases of ion flux modulations observed from AMPTE/CCE.

Azimuthally Polarized Magnetic Pulsations

Figure 4 shows magnetic field and ion flux data associated with a magnetic pulsation polarized in the east–

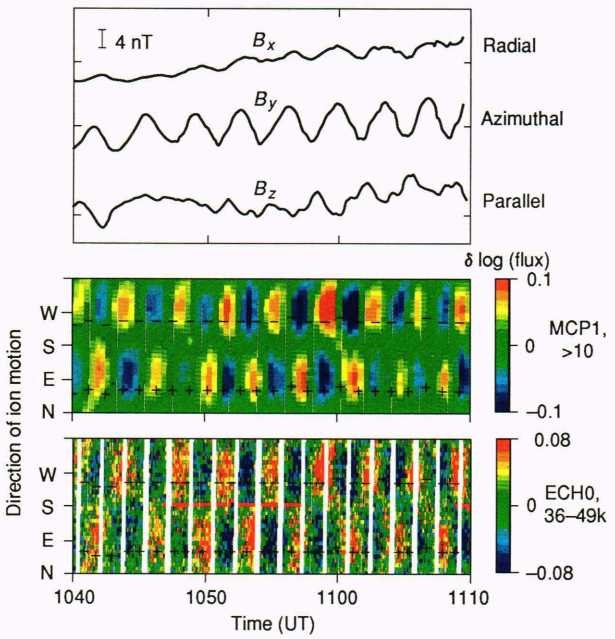

Figure 4. Magnetic field and ion data for an azimuthally polarized magnetic pulsation. To enhance the modulation of ion fluxes, the slowly changing background was defined by taking sliding averages in each sector and subtracting them from the original time series.

west direction. The perturbation in the flux intensity of the particles is displayed in color as a function of time and the detector look direction. Strong flux modulations with the same periodicity as the magnetic pulsation occur in the sectors detecting ions moving eastward (E) or westward (W). The oscillations in these sectors are in antiphase, however, and with respect to B_y the oscillations have a phase difference of $\pm 90°$. There is no phase difference between MCP1 and ECH0.

To understand the flux oscillations, we first consider the fluid-like behavior of the plasma for the wave. The azimuthal polarization and the long period (200 s) of the magnetic pulsation indicate that it is a fundamental-mode standing Alfvén wave and is excited by a large-scale (in azimuthal dimension) external pressure variation. For this mode, the plasma motion is also in the azimuthal direction and its amplitude is maximum at the equator. The velocity oscillation should be in quadrature with B_y, as can be understood from Figure 1.

A plasma consists of many particles, and their velocity distribution has a finite thermal spread, as shown by the solid curve in Figure 5. The fluid velocity is defined as the average of the distribution. As the detector spins, the distribution is sampled twice in v_y, at $v_y = \pm(2W/M)^{1/2}$, as indicated by two vertical lines. If the plasma is stationary, the fluxes measured at these points are equal. If there is an oscillation of the plasma, however, the distribution is shifted back and forth. The consequence is antiphase oscillations in the fluxes at the two velocity points. This model also explains why there is no phase lag between measurements at different energies. In relation to Equation 3, the flux modulation mechanism can be expressed as

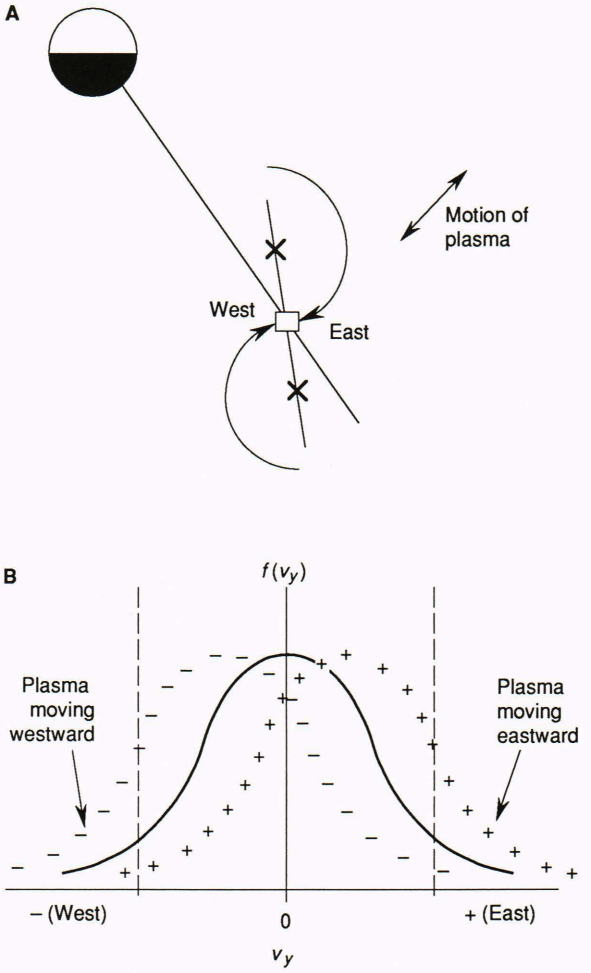

Figure 5. Analysis of the pulsation event in Figure 4. **A.** Geometry of ion measurements. **B.** Schematic of the modulation of ion distribution function by the pulsation.

$$\delta f = -\left(\frac{\partial f}{\partial W}\right)\delta W \ , \tag{4}$$

with

$$\delta W \approx M v_y \, \delta V \ , \tag{5}$$

where δV is the wave-induced perturbation in the fluid velocity. Because δW is related to the local electric field as $\delta V \approx E/B$, the particle data can be used to determine the electric field of magnetic pulsations.[17,18]

This type of particle flux modulation is very common with magnetic pulsations excited by large-scale external pressure variations. What exactly constitutes the pressure variations, however, is still a matter of debate.[19,20]

Radially Polarized Magnetic Pulsations

An example of another type of transverse magnetic pulsations, also often observed by CCE,[17,21] is shown in Figure 6. The location of CCE and the geometry for the event is illustrated in Figure 7. This pulsation is characterized by a radial field oscillation and is accompanied

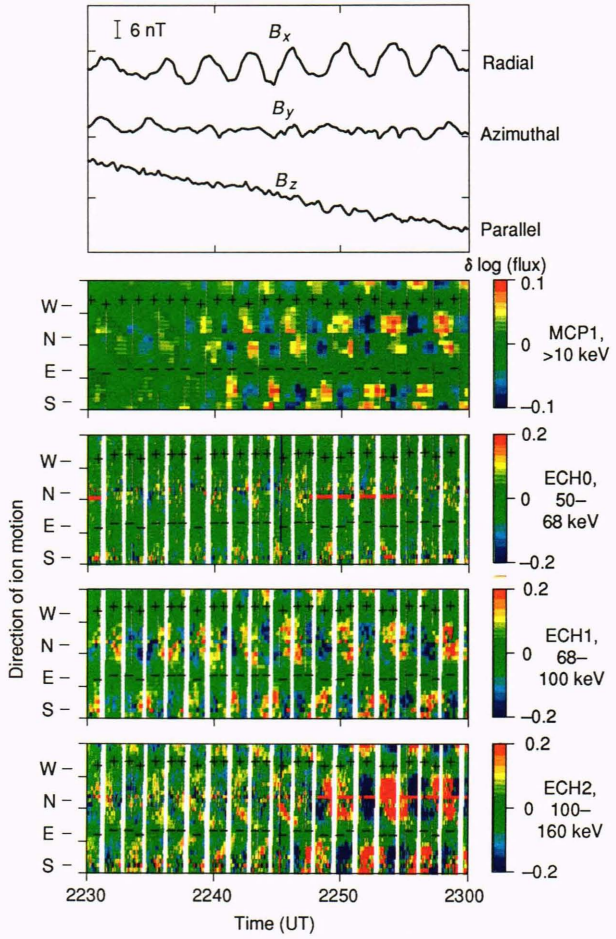

Figure 6. Magnetic field and particle data for a radially polarized Pc 5 magnetic pulsation.

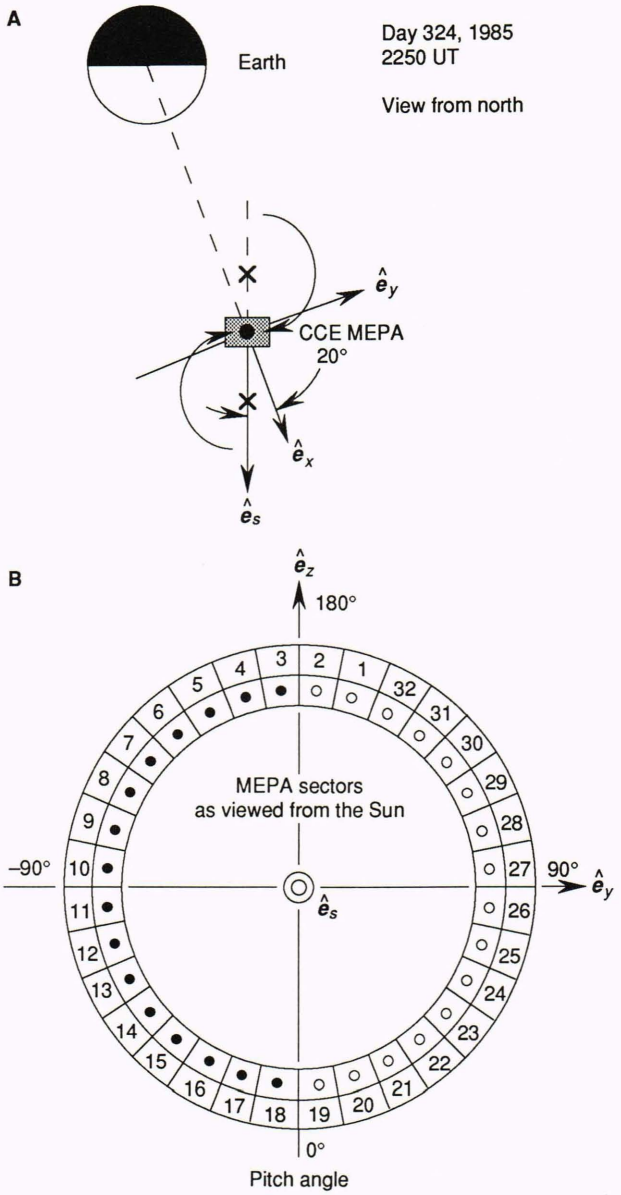

Figure 7. Ion measurements for the event in Figure 6. **A.** The geometry of the event. **B.** MEPA sector definition. The unit vectors $\mathbf{e}_x$, $\mathbf{e}_y$, and $\mathbf{e}_z$ are directed in the radial, eastward, and northward directions respectively, and $\mathbf{e}_s$ is the direction of spacecraft spin. (Reprinted, with permission, from Ref. 22: © 1990 American Geophysical Union.)

by ion flux oscillations that are different from the above example: The amplitude of flux oscillations maximizes near north (N) and south (S) sectors, and the oscillation phase is energy-dependent.

The flux oscillation arises because some particles, but not the entire plasma, drift at a velocity comparable to the azimuthal phase velocity of the pulsation and thus are nearly in resonance with the wave. To understand the response of particles, both the azimuthal and field-aligned structure of the pulsation must be considered. The strong transverse oscillation observed near the magnetic equator indicates that the pulsation has a second-harmonic standing structure. The radial magnetic field oscillation indicates an electric field perturbation in the azimuthal direction, the same direction as guiding center drift.

If we assume that the wave propagates in the azimuthal direction while it is standing along the geomagnetic field, then the electric field of the pulsation should have a spatial pattern as illustrated in Figure 8. The zigzag lines included in this figure are the schematic guiding center orbits of ions that are in resonance with the wave. These particles see an electric field of the same sign as they bounce and drift, and hence they are subject to large acceleration or deceleration. The energy modulation experienced by the ions, regardless of whether or not they are in resonance with the wave, is given by

$$\delta W = \int_{\text{orbit}} qE_y V_{dy}\, dt\ , \tag{6}$$

where V_{dy} is the azimuthal component of ion-guiding-center drift velocity. As before, the corresponding flux modulation is given by

$$\delta f = -\left(\frac{\partial f}{\partial W}\right)\delta W\ . \tag{7}$$

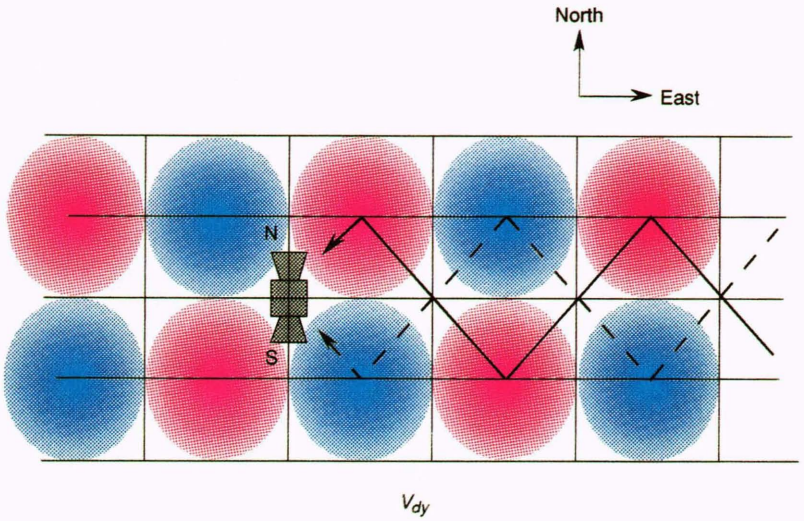

Figure 8. Schematic of the orbits of ion guiding centers and the electric field structure of a second-harmonic standing wave.

Because V_{dy} depends on energy, only particles in a limited energy band experience a large energy modulation. As is the case with other resonant phenomena, the oscillation phase depends on whether particles are drifting slower than the wave, with the wave, or faster than the wave. This explains why there is a shift in oscillation phase with energy. For the magnetic pulsation shown, standing wave structure must be also considered when taking the integral (Eq. 6). If that is done, one finds that resonance occurs when

$$(\omega - m\omega_d)^2 - \omega_b^2 = 0 \qquad (8)$$

is satisfied, where ω_d is the azimuthal drift frequency and ω_b is the bounce frequency of the particles. Both ω_d and ω_b depend on particle energy. This fact has been used to determine the azimuthal wave number from the observed energy-dependent phase of a magnetic pulsation, and $m \sim -100$ (westward propagation) was inferred.[22]

Also, for a given energy, whether particles are accelerated or decelerated depends on whether they enter the detector from the north or from the south. This explains the antiphase oscillations in the N and S sectors.

Another type of phase lag occurs between the fluxes of particles with the same energy and pitch angle but with different guiding center locations. An example is shown in Figure 9. The oscillation phase of the flux of particles with eastside guiding centers (eastside wave) leads the westside wave. This occurs because the pulsation propagates westward and has an azimuthal wavelength, λ_y, not much larger than the radius of gyromotion, ρ, of the particles. The two traces in Figure 9 thus represent the phase of field variation evaluated at the two guiding centers (marked $\times$ in Fig. 7). The azimuthal wavelength; the time lag, Δt, between the eastside and westside fluxes; the period of the pulsation, T; and the

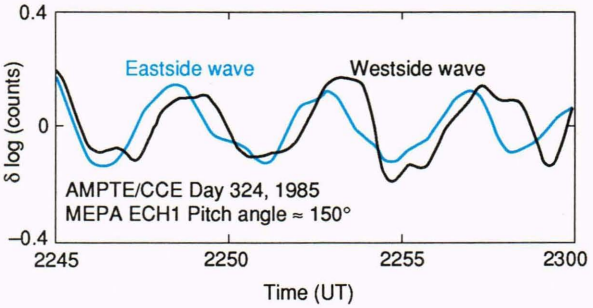

Figure 9. Comparison of the oscillations of ion fluxes corresponding to azimuthally separated guiding centers. (Reprinted, with permission, from Ref. 22: © 1990 American Geophysical Union.)

azimuthal separation of the guiding centers, Δy_G, are related as

$$\frac{\Delta y_G}{\lambda_y} \sim \frac{\Delta t}{T} . \qquad (9)$$

This relationship has been used to determine the propagation direction and azimuthal wave number of pulsations.[23–26] For the case shown in Figure 9, the phase lag is consistent with westward propagation, as inferred above. The westward propagation and large azimuthal wave number suggest that the radially polarized waves are generated by energetic ions as they diffuse outward at the outer edge of the ring current.[7,27]

Compressional Magnetic Pulsations

Compressional magnetic pulsations modulate the flux of energetic particles in yet another way. When the particle gyroperiod is shorter than the wave period, and its gyroradius is smaller than the spatial scale of the wave, the magnetic moment, μ, is conserved for each particle. When particle acceleration is not effective during a com-

pressional magnetic oscillation, particles keep μ constant by changing their pitch angles. To find out how particles respond under these conditions, consider α in the range of 0° to 90°. If $\delta B_z > 0$, then $\delta\alpha > 0$, and vice versa. Next assume that the average pitch angle distribution peaks at 90°, as illustrated by the solid curve in Figure 10. If a flux measurement is made at a pitch angle α_M, particles entering the detector when $\delta B_z > 0$ had a pitch angle smaller than α_M when the wave was not present (i.e., $\delta B_z = 0$). Then, from the Liouville theorem, it follows that the flux decreases at α_M. The opposite happens when $\delta B_z > 0$. The flux changes for $\alpha = 90°$ to 180° are just the mirror image of those for $\alpha = 0°$ to 90°. In terms Equation 3, this can be summarized as

$$\delta f \sim -\frac{\tan\alpha}{2}\frac{\partial f}{\partial \alpha}\frac{\delta B_z}{B_z} \quad . \tag{10}$$

Because this effect occurs at all α_M, the pitch angle distribution changes with ΔB_z, as illustrated in the two additional traces in Figure 10. This explains the major feature of ion flux oscillations in Figure 11.

Although the mirror effect alone does not carry information about propagation direction, the finite Larmor radius effect (Eq. 9) is also observable during compressional ULF wave events, and it is possible to determine the spatial structure of the waves from particle measurements.[22,25]

CONCLUSION

We have outlined the linear response of energetic ions to ULF pulsations and have related the dynamics of individual particles to modulations in particle fluxes that can be measured. Using examples from the AMPTE/CCE spacecraft, we have shown different types of ion flux modulations and have demonstrated in each example that the particle data provide us with information on the waves that cannot be obtained from magnetic field measurements alone. In a sense, the particles can be considered as a remote sensing tool. Because multisatellite observations are not readily available, the techniques described here are extremely useful for studying ULF waves in the magnetosphere. Finally, for more mathematically rigorous treatment of the above particle flux oscillations, readers are referred to a series of papers by Southwood and Kivelson.[28-31]

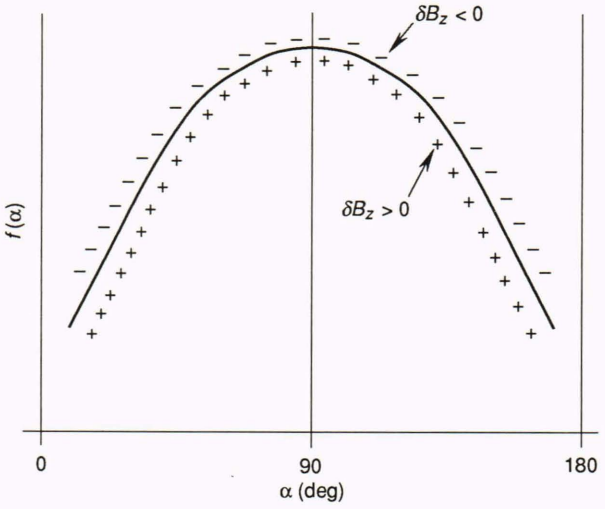

Figure 10. Magnetic field and particle data for a compressional Pc 5 wave.

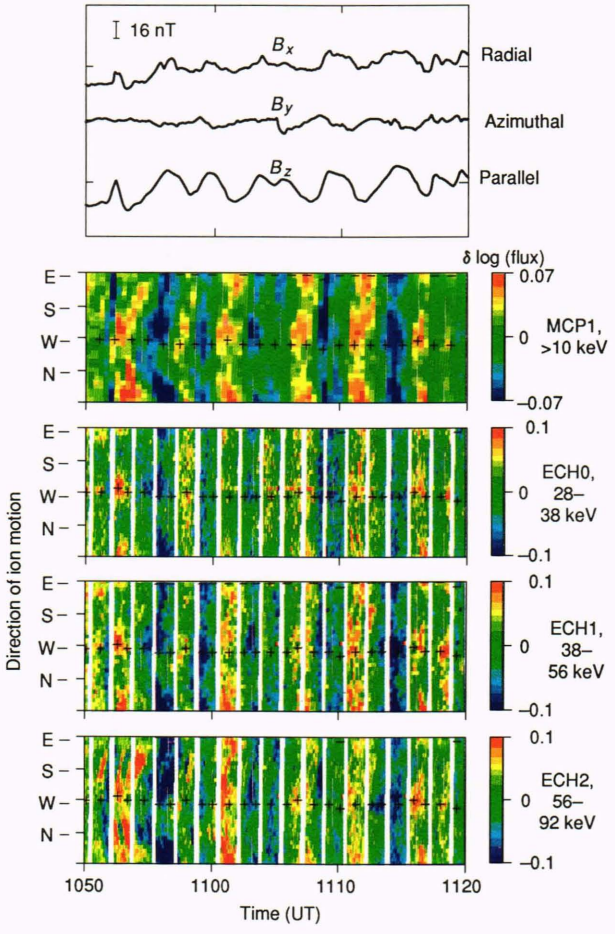

Figure 11. Schematic for ion flux modulations as a function of pitch angle during a compressional Pc 5 wave.

REFERENCES

[1] Stewart, B., "On the Great Magnetic Disturbance Which Extended from August 28 to September 7, 1859, as Recorded by Photography at the Kew Observator," *Phil. Trans. Roy. Soc.* London, p. 425 (1861).

[2] Dungey, J. W., *Electrodynamics of the Outer Atmosphere*, Ionospheric Research Laboratory, Report No. 69, Pennsylvania State University, University Park, Pa., pp. 1-52 (1954).

[3] Judge, D. L., and Coleman, P. J., Jr., "Observations of Low-Frequency Hydromagnetic Waves in the Distant Geomagnetic Field, Explorer 6," *J. Geophys. Res.* **67**, 5071-5090 (1962).

[4] Chen, L., and Hasegawa, A., "A Theory of Long-Period Pulsations, 1, Steady State Excitation of Field Line Resonances," *J. Geophys. Res.* **79**, 1024-1032 (1974).

[5] Southwood, D. J., "Some Features of Field Line Resonances in the Magnetosphere," *Planet. Space Sci.* **22**, 483-491 (1974).

[6] Hasegawa, A., "Drift Mirror instability in the Magnetosphere," *Phys. Fluids* **12**, 2642-2650 (1969).

[7] Southwood, D. J., "A General Approach to Low-Frequency Instability in the Ring Current Plasma," *J. Geophys. Res.* **81**, 3340-3348 (1976).

[8] Takahashi, K., Fennell, J. F., Amata, E., and Higbie, P. R., "Field-Aligned Structure of the Storm Time Pc 5 Wave of November 14-15, 1979," *J. Geophys. Res.* **92**, 5857-5864 (1987).

[9]Takahashi, K., and McPherron, R. L., "Harmonic Structure of Pc 3-4 Pulsations, *J. Geophys. Res.* **87**, 1504–1516 (1982).
[10]Sonnerup, B. U. O., Cahill, L. J., Jr., and Davis, L. R., "Resonant Vibration of the Magnetosphere Observed from Explorer 26," *J. Geophys. Res.* **74**, 2276–2288 (1969).
[11]Kokubun, S., Kivelson, M. G., McPherron, R. L., and Russell, C. T., "OGO 5 Observations of Pc 5 Waves: Particle Flux Modulations," *J. Geophys. Res.* **82**, 2774–2784 (1977).
[12]Su, S.-Y., McPherron, R. L., Konradi, A., and Fritz, T. A., "Observations of ULF Oscillations in the Ion Fluxes at Small Pitch Angles with ATS 6," *J. Geophys. Res.* **85**, 515–522 (1980).
[13]Southwood, D. J, "The Behavior of ULF Waves and Particles in the Magnetosphere," *Planet. Space Sci.* **21**, 53–65 (1973).
[14]Potemra, T. A., Zanetti, L. J., and Acuña, M. H., "The AMPTE/CCE Magnetic Field Experiment," *ISEE Trans. Geosci. Remote Sensing* **GE-23**, 246–249 (1985).
[15]Takahashi, K., Anderson, B. J., and Strangeway, R. J., "AMPTE CCE Observations of Pc 3-4 Pulsations at L = 2–6," *J. Geophys. Res.* **95**, 17179–171786 (1990).
[16]McEntire, R. W., Keath, E. P., Fort, D. E., Lui, A. T. Y., and Krimigis, S. M., "The Medium-Energy Particle Analyzer (MEPA) on the AMPTE/CCE Spacecraft," *IEEE Trans. Geosci. Remote Sensing* **GE-23**, 230–233, (1985).
[17]Takahashi, K., Kistler, L. M., Potemra, T. A., McEntire, R. W., and Zanetti, L. J., "Magnetospheric ULF Waves Observed During the Major Magnetospheric Compression of November 1, 1984," *J. Geophys. Res.* **93**, 14,369–14,382 (1988).
[18]Mitchell, D. G., Engebretson, M. J., Williams, D. J., Cattell, C. A., and Lundin, R., "Pc 5 Pulsation in the Outer Dawn Magnetosphere Seen by ISEE-1 and -2," *J. Geophys. Res.* **95**, 967–975 (1990).
[19]Potemra, T. A., Luehr, H., Zanetti, L. J., Takahashi, K., Erlandson, R. E., et al., "Multisatellite and Ground-Based Observations of Transient ULF Waves," *J. Geophys. Res.* **94**, 2543–2554 (1989).
[20]Sibeck, D. G., Baumjohann, W., Elphic, R. C., Fairfield, D. H., Fennell, J. F., et al., "The Magnetospheric Response to 8-Minute-Period Strong-Amplitude Upstream Pressure Variations," *J. Geophys. Res.* **94**, 2505–2519 (1989).
[21]Engebretson, M. J., Zanetti, L. J., Potemra, T. A., Klumpar, D. M., and Acuña, M. H., "Observations of Intense ULF Pulsation Activity Near the Geomagnetic Equator During Quiet Times," *J. Geophys. Res.* **93**, 12,795–12,816 (1988).
[22]Takahashi, K., McEntire, R. W., Lui, A. T. Y., and Potemra, T. A., "Ion Flux Oscillations Associated with a Radially Polarized Transverse Pc 5 Magnetic Pulsation," *J. Geophys. Res.* **95**, 3717–3731 (1990).
[23]Takahashi, K., Lopez, R. E., McEntire, R. W., Zanetti, L. J., Kistler, L. M., and Ipavich, F. M., "An Eastward Propagating Compressional Pc 5 Wave Observed by AMPTE/CCE in the Postmidnight Sector," *J. Geophys. Res.* **92**, 13,472–13,484 (1987).
[24]Kremser, G., Korth, A., Fejer, J. A., Wilken, B., Gurevich, A. V., and Amata, E., "Observations of Quasi-Periodic Flux Variations of Energetic Ion and Electrons Associated with Pc 5 Geomagnetic Pulsations," *J. Geophys. Res.* **86**, 3345–3356 (1981).
[25]Lin, N., McPherron, R. L., Kivelson, M. G., and Williams, D. J., "An Unambiguous Determination of the Propagation of a Compressional Pc 5 Wave," *J. Geophys. Res.* **93**, 5601–5612 (1988).
[26]Takahashi, K., Cheng, C. Z., McEntire, R. W., and Kistler, L. M., "Observation and Theory of Pc 5 Waves with Harmonically Related Transverse and Compressional Components," *J. Geophys. Res.* **95**, 977–989 (1990).
[27]Chen, L., and Hasegawa, A., "On Magnetospheric Hydromagnetic Waves Excited Energetic Ring Current Particles," *J. Geophys. Res.* **93**, 8763–8767 (1988).
[28]Southwood, D. J., and Kivelson, M. G., "Charged Particle Behavior in Low-Frequency Geomagnetic Pulsations, 1, Transverse Waves," *J. Geophys. Res.* **86**, 5643–5655 (1981).
[29]Southwood, D. J., and Kivelson, M. G., "Charged Particle Behavior in Low-Frequency Geomagnetic Pulsations, 2, Graphical Approach," *J. Geophys. Res.* **87**, 1707–1710 (1982).
[30]Kivelson, M. G., and Southwood, D. J., "Charged Particle Behavior in Low-Frequency Geomagnetic Pulsations, 3, Spin Phase Dependence," *J. Geophys. Res.* **88**, 174–182 (1983).
[31]Kivelson, M. G., and Southwood, D. J., "Charged Particle Behavior in Low-Frequency Geomagnetic Pulsations, 4, Compressional Waves," *J. Geophys. Res.* **90**, 1486–1498 (1985).

ACKNOWLEDGMENTS: This article summarizes several articles published in the last few years reporting on AMPTE/CCE observations. The author gratefully acknowledges the contribution of the authors of those publications: Brian J. Anderson, Ramon E. Lopez, Anthony T. Y. Lui, Richard W. McEntire, Thomas A. Potemra, and Lawrence J. Zanetti of APL, Frank Cheng of the the Princeton Plasma Physics Laboratory, and Lynn M. Kistler of the University of Maryland. The author thanks Stuart R. Nylund of APL for software support. This work was supported by NASA under Task I of Navy Contract N00039-89-C-5301.

THE AUTHOR

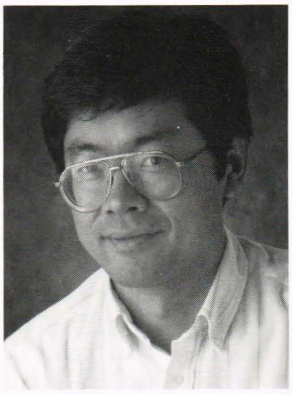

KAZUE TAKAHASHI was born in Japan in 1954. He received B.S. and M.S. degrees from Tohoku University, came to the United States in 1978, and received a Ph.D. in geophysics and space physics from UCLA in 1983. After spending three years at the Los Alamos National Laboratory as a postdoctoral fellow, he joined APL in 1986 where he is on the Senior Professional Staff in the Space Physics Group. His main research interests are ULF waves and substorms in the magnetosphere. He is currently analyzing magnetic field and energetic particle data from the AMPTE/CCE spacecraft to understand the generation and propagation of ULF waves in the magnetosphere and to understand the temporal development of substorm-associated current systems in the magnetotail.